A Benefit of Multiple Carrier GNSS Signals: Regional Scale Network-Based RTK with Doubled Inter-Station Distances

Yanming Feng[1] Bofeng Li[1, 2]

[1:] Faculty of Information Technology, Queensland University of Technology, GPO Box 2434, QLD 4001, Australia
[2:] Department of Surveying and Geo-informatics Engineering, Tongji University, Shanghai 200092, P.R. China

Abstract. This paper presents a regional scale network-based real time kinematic positioning strategy based on use of three carrier GNSS signals, in which the inter-station distances of the network could be doubled, that is, around 140 to 180 km instead of the current 70 to 90 km with the use of dual-frequency GPS receivers. The paper outlines the most efficient virtual observables and models that allow for resolving ambiguities of three carriers with observation of above 7 minutes for the baselines of a few hundreds of kilometres. As a result, the remaining key limiting factor for implementation of the regional scale network RTK is the distance-dependent residual tropospheric bias. A reference station placement scheme of doubling the inter-station distances is then suggested based on interpolation accuracy of the tropospheric errors within the network. A semi-simulation procedure is introduced for generation of the third GPS signals from the real GPS L1 and L2 data to allow for more subjective assessment of TCAR performance benefits in the real world situations. Numerical studies performed with the 24-h data sets from four US CORS stations have demonstrated superior AR performance benefits of the outlined TCAR algorithms, providing the technical basis for the deployment of regional scale network RTK services with doubled inter-station distances. The distance-independent nature of the AR performance has significant implications for the future GNSS technological evolutions and applications.

Keywords. GNSS, Three Carrier Ambiguity Resolution, Network RTK

1. Introduction

The key limitation of the existing dual-frequency based real time kinematic (RTK) positioning systems is that the service distance between a reference station and receiver must be kept within a few tens of kilometres. This is why the rapid and reliable carrier phase ambiguity resolution (AR) becomes more and more difficult when the inter-receiver distance grows longer. This phenomenon is mainly caused by the effects of distance-dependent biases, such as orbital error, ionospheric and tropospheric delays in the double differenced (DD) measurements, or to be precise, distance-dependent characteristics of the these bias or residual terms. As a result, designers of a RTK system have restricted the base-rover distance to about 10 to 20 km or less in the single-base RTK case (Rizos & Han, 2003). In current network-RTK implementations with the virtual reference station (VRS) techniques (Chen et al., 2001; Zhang & Lachapelle, 2001), the inter-station distance is typically 70 to 90 km. Hence, the network-based RTK has resulted in a reduction of the investment costs necessary to start a RTK positioning service, since the number of reference stations can be reduced basically by 3 to 4 times. For instance, about 10 reference stations are needed to cover the medium city with area of about 10,000 square kilometres using the 20km single-based RTK system, while deployment of the VRS system of 3 to 4 reference stations may provide services in the same coverage. However, such networks can be available mostly in developed areas with high population density and excellent internet and mobile communication infrastructures. The SunPOZ real-time GPS service, for example, is currently limited to south east Queensland and the five station SunPOZ network covers the area of about 11,000 square kilometres (Cislowski & Higgins, 2006). Nevertheless, if the coverage of the SunPOZ network were extended only to cover inhabited area in Queensland at this density, the number of reference stations would be 150 to 200, costing over ten millions of dollars in installation and significant amount for annual operations.

Future Global Navigation Satellite Systems (GNSS) and augmentations, such as the US modernized Global Positioning System (GPS), the European Galileo system, the Japanese Quasi-Zenith Satellite Systems (QZSS) and the Chinese COMPASS system, all operate with three or more frequencies, as outlined in Table 1. Significant research

efforts have been made in the past ten years to make use of the third GNSS signals to improve RTK services, including the early contributions by Forssell et al (1997),Vollath et al (1998), Han & Rizos (1999), De Jonge et al. (2000), Hatch et al (2000), Teunissen et al (2002), Vollath (2004) and Henkel and Cünther (2007). Recent efforts by Feng & Rizos (2005), Feng and Moody (2006), Hatch (2006), Feng and Rizos (2007) and Feng (2008) have specifically examined the performance potential of multiple-frequency GNSS signals on the reliable AR over longer inter-receiver distances, resulting in some promising findings. Given three L-band frequencies, one can generally identify the three best virtual observables to allow for more reliable AR under the given observational conditions characterized by the magnitudes of ionospheric activity, tropospheric condition, phase noise and orbital error. The selected virtual observables often have minimum or low ionospheric effects, and are thus referred to as ionosphere-reduced virtual observables. As a result, the effects of the ionospheric biases in the geometry-based observation models can be significantly mitigated even eliminated for the long baselines, such as those over tens to hundreds of kilometres in length.

Table 1: GPS, Galileo, Glonass, Compass and QZSS frequencies (unit: MHz)

System	**L1**	**E1**	**E2**	**L2**	**E6**	**E5B**	**E5A/L5**
Modernized GPS	1575.42			1227.40			1176.45
Galileo	1575.42				1278.750	1207.140	1176.45
Glonass	1598.0625-1609.3125			1242.9375-1251.6875			
Compass/Beidou		1589.742	1561.098		1268.52	1207.140	
QZSS	1575.42			1227.40			1176.45

Due to lack of the third frequency data, the above performance benefits from using multiple GNSS signals were understood from theoretical analysis and numerical analysis with simulated three frequency data. The problem is that simulated GNSS data sets are based on the operator's assumptions instead of real world situations, for variations of different biases and uncertainty degrees of different error sources. To overcome this problem, Li (2008) proposed a semi-simulation approach for generating the third DD frequency GPS signals from L1 and L2 signals. The key is the separation between effects of ionospheric biases, tropospheric errors and phase noises. The idea is described as follows. First, the integer ambiguities of L1 and L2 frequencies are solved over the network and fixed to their integer values, and then the tropospheric and ionospheric delays are separated using the ionosphere-free and geometry-free measurements, respectively. Finally, the third frequency L5 or E6 signals are generated by substituting the tropospheric biases and their corresponding ionosphere errors into the linear equations, adding the simulated phase noises. This semi-simulation approach is rather convenient and efficient for generation of new DD signals based on the existing dual-frequency GPS data sets and can help the demonstration of network-RTK capability over longer inter-station baselines with multiple frequencies.

This paper outlines a regional area network-based RTK strategy based on the use of three carrier GNSS signals, in which the inter-station distances of the network is doubled, that is, from 140 to 180 km instead of the current the inter-station distances of 70 to 90 km when the reference stations are equipped with triple frequency GPS receivers. The context is organised as follows. Section 2 introduces the virtual observables and models for geometry-free and geometry-based three carrier ambiguity resolution (TCAR) processes, which allow for solving ambiguities of three carriers over the distance of a few hundreds of kilometres between continuously operating reference stations (CORS). Section 3 examines the reference station placement scheme by doubling the inter-station distances based on the long-range AR capacity achievable with triple frequency measurements. Section 4 outlines the semi-simulation procedure that can generate the third and fourth GPS signals from the real GPS L1 and L2 data. Section 5 provides numerical analyses performed with three 24-h data sets from the US CORS network to demonstrate the performance benefits of the outlined TCAR algorithms. The final section gives a summary of the findings of the paper.

2. Geometry-free and geometry-based models for TCAR

We start with definitions of general observation equation for a virtual phase GPS signal,

$$\phi_{(i,j,k)} = \rho + \delta_{orbit} + c(\delta t_S - \delta t_R) + \delta_{trop} - \beta_{(i,j,k)} \frac{K_1}{f_1^2} - \lambda_{(i,j,k)}[\varphi_S^0 - \varphi_R^0 + N]_{(i,j,k)} + \varepsilon_{\phi(i,j,k)} \quad (1)$$

and the virtual code observable is,

$$P_{(l,m,n)} = \rho + \delta_{orbit} + c(\delta t_S - \delta t_R) + \delta_{trop} + \beta_{(l,m,n)} \frac{K_1}{f_1^2} + \varepsilon_{P(l,m,n)} \quad (2)$$

In both Eqs (1) and (2), ρ is the geometric distance between satellite S and receiver antenna R; c is the speed of light in vacuum; δ_{orbit} is the satellite orbital error in metres; δt_R is the receiver clock error of all components in seconds; δt_S is the satellite clock error of all components in seconds; δ_{trop} is the tropospheric propagation delay in metres; K_1/f_1^2 is the ionospheric delay at L1 carrier; φ_S^0 is the initial phase of the satellite oscillator in cycles, which is satellite-dependent; φ_R^0 is initial phase of the oscillator in cycles, which is receiver-dependent; $\varepsilon_{\phi(i,j,k)}$ is the observation noise including the effects of the high-order ionospheric error and multipath (Kim & Langley, 2007). $\phi_{(i,j,k)}$ is defined as a linear combination of three fundamental observables (Feng & Rizos, 2005; Feng, 2008),

$$\phi_{(i,j,k)} = \frac{i \cdot f_1 \cdot \phi_1 + j \cdot f_2 \cdot \phi_2 + k \cdot f_5 \cdot \phi_5}{i \cdot f_1 + j \cdot f_2 + k \cdot f_5} \quad (3)$$

where i, j, k are integer coefficients; ϕ_i is the phase measurements in metres and f_i is the frequency on L_i carrier for i=1, 2 and 5; l, m, n are also integer coefficients. P_1, P_2 and P_5 are the code measurements on each of the three observables; $P_{(l,m,n)}$ is similarly defined as,

$$P_{(l,m,n)} = \frac{l \cdot f_1 \cdot P_1 + m \cdot f_2 \cdot P_2 + n \cdot f_5 \cdot P_5}{l \cdot f_1 + m \cdot f_2 + n \cdot f_5} \quad (4)$$

$\beta_{(i,j,k)}$ is the first-order ionospheric scale factor (ISF) expressed as,

$$\beta_{(i,j,k)} = \frac{f_1^2 (i/f_1 + j/f_2 + k/f_5)}{i \cdot f_1 + j \cdot f_2 + k \cdot f_5} \quad (5)$$

The variances for phase and code noises $\varepsilon_{\phi(i,j,k)}$ and $\varepsilon_{p(l.m.n)}$ are given by,

$$\sigma^2(\varepsilon_{\phi(i,j,k)}) = \frac{(i \cdot f_1)^2 + (j \cdot f_2)^2 + (k \cdot f_5)^2}{(i \cdot f_1 + j \cdot f_2 + k \cdot f_5)^2} \sigma_{\phi 1}^2 \equiv \mu_{(i,j,k)}^2 \sigma_{\phi 1}^2 \quad (6)$$

and

$$\sigma^2(\varepsilon_{p(i,j,k)}) = \frac{(i \cdot f_1)^2 + (j \cdot f_2)^2 + (k \cdot f_5)^2}{(i \cdot f_1 + j \cdot f_2 + k \cdot f_5)^2} \sigma_{P1}^2 \equiv \mu_{(i,j,k)}^2 \sigma_{P1}^2 \quad (7)$$

The DD phase and code measurements are,

$$\Delta\nabla\phi_{(i,j,k)} = \Delta\nabla\rho + \Delta\nabla\delta_{orbit} + \Delta\nabla\delta_{trop} - \beta_{(i,j,k)} \frac{\Delta\nabla K_1}{f_1^2} - \lambda_{(i,j,k)} \Delta\nabla N_{(i,j,k)} + \varepsilon_{\Delta\nabla\phi(i,j,k)} \quad (8)$$

and

$$\Delta\nabla P_{(l,m,n)} = \Delta\nabla\rho + \Delta\nabla\delta_{orbit} + \Delta\nabla\delta_{trop} + \beta_{(l,m,n)} \frac{\Delta\nabla K_1}{f_1^2} + \varepsilon_{\Delta\nabla p(l,m,n)} \quad (9)$$

where the symbol "$\Delta\nabla$" represents the DD operation applied to the quantity immediately to the right; $\Delta\nabla\rho$ is the computed value of the DD range.

In addition, the linearly combined phase observable has the virtual frequency,

$$f_{(i,j,k)} = i \cdot f_1 + j \cdot f_2 + k \cdot f_5 \quad (10)$$

the virtual wavelength,

$$\lambda_{(i,j,k)} = c/f_{(i,j,k)} \quad (11)$$

and the cycle ambiguity,

$$N_{(i,j,k)} = i \cdot N_1 + j \cdot N_2 + k \cdot N_5 \tag{12}$$

For any three GNSS signals, we will assume the conditions for their frequencies, $f_1 > f_2 > f_5$ and $f_2 - f_5 < f_1 - f_2$.

2.1 Geometry-free TCAR models

The term "geometry-free" refers to the observation model for ambiguity parameters being formed without the term of the geometric distance between receivers and satellites. Geometry-free TCAR directly estimates ambiguity parameters using either code measurements or ambiguity-fixed phase measurements. In the former case, the geometry-free observational model for the integer parameter is given by,

$$\frac{\Delta\nabla P_{(l,m,n)} - \Delta\nabla\phi_{(i,j,k)}}{\lambda_{(i,j,k)}} = \Delta\nabla N_{(i,j,k)} + \varepsilon_{TN} \tag{13}$$

where, $\varepsilon_{TN} = \frac{1}{\lambda_{(i,j,k)}}\{[\beta_{(l,m,n)} + \beta_{(i,j,k)}]\frac{\Delta\nabla K_1}{f_1^2} + \varepsilon_{\Delta\nabla P(l,m,n)} + \varepsilon_{\Delta\nabla\phi(i,j,k)}\}$ and (l, m, n) and (i, j, k) generally represent different groups of integers, thus infinite possible combinations. In this context, we define the combinations with wavelengths longer than 2.93m and between 0.75 and 2.93m as extra-widelane (EWL) and widelane (WL), respectively. Code and phase observables that are minimally affected by the joint ionospheric term, code and phase noises, with respect to their virtual wavelengths, should be considered as the best choices for AR purposes. Three usual choices are the WL $(\Delta\nabla P_{(1,1,0)} - \Delta\nabla\phi_{(1,-1,0)})$ and $(\Delta\nabla P_{(1,0,1)} - \Delta\nabla\phi_{(1,0,-1)})$, as well as EWL $(\Delta\nabla P_{(0,1,1)} - \Delta\nabla\phi_{(0,1,-1)})$, where the ionospheric term in Eq (13) is cancelled, and the effect of the code noise term is nearly minimised. However, considering the effects of all the factors, it is possible to find more useful observables for AR purpose under the different ionospheric and noise conditions. Feng et al (2007) set up a criterion making the total noise level (TNL) in cycles minimal. Then given an appropriate error budget in ε_{TN} of Eq (13) and a preferred choice of virtual code measurements, typically $\Delta\nabla P_{(1,1,0)}$ that is available for any triple frequency systems, one can identify two most useful linearly independent EWL/WL virtual observables. The first one always is the EWL $\Delta\nabla\phi_{(0,1,-1)}$, which has the minimal total noise level. In each GNSS three frequency service there are a few more WL virtual observables, such as $\Delta\nabla\phi_{(1,-4,3)}$ and $\Delta\nabla\phi_{(1,-3,2)}$ having lower total noise levels than that of the traditional WL observable, $\Delta\nabla\phi_{(1,-1,0)}$ and $\Delta\nabla\phi_{(1,0,-1)}$. One can choose to determine the ambiguity for any one of the lower TNL observables along with the first EWL observable through a rounding process, usually taking certain number of epochs to obtain 100% AR success rate (Feng, 2008).

A similar procedure can be performed to find the third virtual observable from a new category, of which any combination is independent of the previous two EWL/WL virtual observables. The problem is that there are no EWL/WL candidates in the new category that allows ambiguity fixing to be carried out as easily as the first two observables. AR with medium-lane (ML, 0.1903 m $<\lambda<$ 0.75m) and narrow-lane (NL, 0.10 m $< \lambda <$ 0.1903 m) observables would suffer heavily from the effects of code noises and the effects of the ionospheric delays. However, it is possible to use an ambiguity-resolved phase observable, $\phi_{(l,m,n)}$, derived from the above EWL/WL category to estimate the ambiguity of the new observable, generally with the following equation,

$$\frac{\Delta\nabla\phi_{(l,m,n)} + \lambda_{(l,m,n)}\Delta\nabla N_{(l,m,n)} - \Delta\nabla\phi_{(i,j,k)} + [\beta_{(l,m,n)} - \beta_{(i,j,k)}]\frac{\Delta\nabla\hat{K}_1}{f_1^2}}{\lambda_{(i,j,k)}} = \Delta\nabla N_{(i,j,k)} + \varepsilon_{TN} \tag{14}$$

where $\varepsilon_{TN} = -\frac{1\Delta K}{\lambda_{(i,j,k)}}\{[\beta_{(l,m,n)} - \beta_{(i,j,k)}]\frac{\nabla\ 1}{f_1^2} - \varepsilon_{\Delta\nabla\phi(l,m,n)} + \varepsilon_{\Delta\nabla\phi(i,j,k)}\}$; $\phi_{(l,m,n)}$, for instance, can be the WL observables $\phi_{(1,-1,0)}$ or $\phi_{(1,0,-1)}$. Considering that the uncertainty of the ionospheric estimate $\Delta\nabla\hat{K}_1/f_1^2$ may be generally derived from an independent method and error dependence between all the noise terms in the analysis, one can similarly compute the total noise levels (in units of cycles) to identify the 'best' useful observable for AR of the third observable. However, unlike the selection of EWL/WL observables in the previous category where a few observables have apparently the lowest total noise level σ_{TN}, there are hundreds of candidates, including the three original

observables, $\phi_{(1,0,0)}$, (L1), $\phi_{(0,1,0)}$ (L2) or $\phi_{(0,0,1)}$ (L5) have near values of TNLs (in cycle). Therefore, any one of the observables may be used to complete the AR process of the third ambiguity.

2.2 Geometry-based TCAR Models

The term "geometry-based" refers to the observation model for ambiguity parameters being formed with the term of the geometric distance between a receiver and a satellite. Geometry-based TCAR makes use of the DD phase observations:

$$\Delta\nabla\phi_{(i,j,k)} = \Delta\nabla\rho + \Delta\nabla\delta_{orbit} + \Delta\nabla\delta_{trop} - \beta_{(i,j,k)}\frac{\Delta\nabla K_1}{f_1^2} - \lambda_{(i,j,k)}\Delta\nabla N_{(i,j,k)} + \varepsilon_{\Delta\nabla\phi(i,j,k)} \quad (15)$$

Referring to Feng (2008), it is possible to identify the three most useful observables for geometry-based TCAR, based on a criterion, for instance, a minimum of the total noise level for Eq (15). Given an appropriate error budgets with respect to the different baseline lengths for all error terms of Eq (15), two most useful EWL/WL and one ML/NL observables for AR with the geometry-based models can be given for any three frequency GNSS case. It is important to note that in each GNSS three frequency service, the EWL and NL choices often have minimal or near minimal ionospheric scale factor. For instance, in the GPS case the EWL observable $\Delta\nabla\phi_{(1,-6,5)}$ and NL $\Delta\nabla\phi_{(4,0,-3)}$ have the ISF values of -0.0744 and -0.0099 and wavelengths of 3.256m and 11.45cm, respectively. As a result, the ionospheric effect in the geometry-based observation models can be eliminated or reduced, thus allowing AR to be performed over the baselines of tens to hundreds of kilometers in length.

2.3 Network-based AR process and performance

In the network-RTK case, the required AR performance at the network centre is different from the AR performance requirement at the user end. The network processing software can make good use of the continuously recording data for AR process and the constraints of known station coordinates, then determine the tropospheric delays with ambiguity-resolved ionosphere-free phase measurements. At the user-end, ideally, the ambiguities can be fixed epoch by epoch, or as few epochs as possible, and the accurately known tropospheric corrections. Therefore, the AR algorithms for the network-based processing and user-based processing could be different. Based on the above virtual observables for geometry-free and geometry-based models, we outline the five-step procedures for the network-based AR processes versus the user-based AR and position estimation (PE) processes in Table 2, considering the cases where all reference stations are equipped with triple frequency receivers and users may use either dual-frequency or triple-frequency receivers. As far as the AR performance in the network-based process is concerned, it can be generally expected that the 100% AR success for all three observables is achievable over hundreds of kilometres using the data of a few epochs to minutes. This has not been possible with dual-frequency based measurements.

3. Reference station placement with doubled inter-station distances

The above analysis indicates that the AR with three carrier observables could be reliably achieved over the inter-station distances of a few hundred kilometres in the network RTK services, which is followed by estimation of the ionospheric and tropospheric biases in DD phase measurements to form grid corrections. However, in order to specify to what degree that the inter-station distances can be extended, care has to be taken to effects of residual ionospheric and tropospheric errors on the rover user terminals anywhere within the network coverage. In the operation of network-RTK systems, the precisely predicted GPS orbits, such as ultra-rapid orbits, are available in real time to replace the broadcast GPS ephemerides, and the effect of orbit errors is no longer of concerns (Kim & Langley, 2007).

The residual ionospheric errors after correction through interpolation of the ionospheric biases can still remain distance-dependent and random in the DD phase measurements of between a user and its nearest or virtual base station. With triple-frequency measurements, the ionospheric term may be corrected at user end to the accuracy of centimetres, to become almost distance-independent (Feng, 2008). With dual-frequency measurements, for instance, i.e., L1 and L2 or L1 and L5, the effect of the residual ionospheric errors reaches the minimum with the ionosphere-reduced virtual observables, such as $\phi_{(4,-3,0)}$ or $\phi_{(4,0,-3)}$, relative to wavelength. As a result, the AR at user-end can tolerate larger ionospheric errors.

Table 2. Network-based computations versus user-based computation

Network-based computation	User-based computation
Step 1: Determination of the first EWL ambiguity using the geometry-free model (13) for the best EWL observable, the AR is computed using measurements from single or a few epochs: $$\Delta\nabla N_{(0,1,-1)} = \left[\frac{\Delta\nabla P_{(0,1,1)} - \Delta\nabla\phi_{(0,1,-1)}}{\lambda_{(0,1,-1)}}\right]_{round} \quad (16)$$ In the case of P5 code unavailable $P_{(1,1,0)}$ can be used instead with the similar performance. Comment: *The 100% AR success of the first EWL observable is achievable with single or a few epochs of observables*.	
Step 2: Formation of the geometry-based linear equation for the second best EWL observables from single or a few epochs, for instance, $\Delta\nabla N_{(1,-6,5)}$ for $\Delta\nabla\phi_{(1,-6,5)}$, can be expressed as $$\Delta\nabla P_{(1,1,0)} = \Delta\nabla\rho + \varepsilon_{\Delta\nabla P_{IF}}$$ $$\Delta\nabla\phi_{(1,-6,5)} = \Delta\nabla\rho - \beta_{(1,-6,5)}\frac{\Delta\nabla K_1}{f_1^2} - \lambda_{(1,-6,5)}\Delta\nabla N_{(1,-6,5)} + \varepsilon_{\Delta\nabla\phi(1,-6,5)} \quad (17)$$ Using the AR method, such as LAMBDA method to resolve the ambiguity $\Delta\nabla N_{(1,-6,5)}$. After the first two EWL ambiguities, $\Delta\nabla N_{(0,1,-1)}$ and $\Delta\nabla N_{(1,-6,5)}$ or their derivatives, including the WL $\Delta\nabla N_{(1,-1,0)}$ and $\Delta\nabla N_{(1,0,-1)}$ are determined. Comment: *The 100% AR success of the second EWL observable in Step 2 with the geometry-free model should be also achievable with normally single epoch to a few epochs over long distances.*	
Step 3: Estimation of the ionospheric delay with the ambiguity resolved $\Delta\nabla\phi_{(0,1,-1)}$ and $\Delta\nabla\phi_{(0,1,-1)}$, $$\Delta\nabla\delta\hat{I} = \frac{f_2 f_5}{f_1(f_2 - f_5)}[(\Delta\nabla\phi_{(1,0,-1)} + \lambda_{(1,0,-1)}\Delta\nabla N_{(1,0,-1)})$$ $$-(\Delta\nabla\phi_{(1,-1,0)} + \lambda_{(1,-1,0)}\Delta\nabla N_{(1,-1,0)}] \quad (18)$$ This estimation has the noise of $83\,\sigma_{\Delta\nabla\phi 1}$ in the GPS case (Feng,2008), but can be refined through smoothing process with the precise ionosphere delay $$\frac{\Delta\nabla K_1}{f_1^2} = \frac{f_2^2}{f_1^2 - f_2^2}(\Delta\nabla\phi_{(1,0,0)} - \Delta\nabla\phi_{(0,1,0)}) \quad (19)$$ *Comment: a RMS accuracy of a few centimetres should be achievable within a few minutes of observations as shown in Fig 4.*	**Step 3:** **Case 1: Dual-frequency users** Interpolation of both ionospheric and tropospheric corrections for user locations, which are delivered to users for AR and position estimation in Step 5. **Case 2: Triple frequency users** Interpolation of the tropospheric corrections for user locations, smoothing the ionospheric estimates from EWL observables as the left, and refining the WL measurements with smoothed ionospheric correction for AR in Step 4.
Step 4: With the smoothed ionospheric delay estimation obtained in Step 3 and the refined WL with the geometry-free model over m epochs, $$\Delta\nabla\tilde{N}_{(1,0,0)} = \left[\frac{1}{m}\sum_1^m \frac{\Delta\nabla\phi_{(1,-1,0)} + \lambda_{(1,-1,0)}\Delta\nabla\tilde{N}_{(1,-1,0)} - \Delta\nabla\phi_{(1,0,0)} + [\beta_{(1,-1,0)} - \beta_{(1,0,0)}]\frac{\Delta\nabla\hat{K}_1}{f_1^2}}{\lambda_{(1,0,0)}}\right]_{round} \quad (20)$$ The estimate (18) is substituted into (20) without smoothing, then taking average of the estimate over m epochs to achieve 100% AR success in (20). *Comment: It is expectable that 100% AR success is achievable over a certain period of observation, for instance 5 to 10 minutes. This performance is distance independent, suitable for network-based AR process.*	**Step 4**: Geometry-based AR **Case 1: Dual-frequency users or single-based RTK** $$\begin{bmatrix}\Delta\nabla P_{(1,1)} - \Delta\nabla\rho_0 \\ \Delta\nabla\phi_{(1,-1)} - \Delta\nabla\rho_0 \\ \Delta\nabla\phi_{(4,-3)} - \Delta\nabla\rho_0\end{bmatrix} = \begin{bmatrix}A & 0 & 0 \\ A & -\lambda_{(1,-1)} & 0 \\ A & 0 & -\lambda_{(4,-3)}\end{bmatrix}\begin{bmatrix}\delta X \\ \Delta\nabla N_{(1,-1)} \\ \Delta\nabla N_{(4,-3)}\end{bmatrix} = \begin{bmatrix}\varepsilon_{\Delta\nabla P(1,1)} \\ \varepsilon_{\Delta\nabla\phi(1,1)} \\ \varepsilon_{\Delta\nabla\phi(4,-3)}\end{bmatrix} \quad (21)$$ where, **A** is the design matrix for parameter δX. Comment: *Comparing to the direct use of L1 and L2 observables, this model is less sensitive to ionospheric errors/biases, but more sensitive to the tropospheric biases.* **Case 2: Triple frequency users** $$\begin{bmatrix}\Delta\nabla\phi_{(1,0,-1)} + \lambda_{(1,0,-1)}\Delta\nabla N_{(1,0,-1)} - \Delta\nabla\rho_0 \\ \Delta\nabla\phi_{(1,0,0)} - \Delta\nabla\rho_0\end{bmatrix} = \begin{bmatrix}A & 0 \\ A & -\lambda_{(1,0,0)}\end{bmatrix}\begin{bmatrix}\delta X \\ \Delta\nabla N_{(1,0,0)}\end{bmatrix} = \begin{bmatrix}\varepsilon_{\Delta\nabla\phi(1,0,-1)} \\ \varepsilon_{\Delta\nabla\phi(1,0,0)}\end{bmatrix} \quad (22)$$ Comment: *This model uses the ionosphere delay corrected measurements (via Step 3), and is less sensitive to tropospheric errors.*
Step 5: Estimation of ionospheric grid corrections using all-resolved L1 and L2 phase measurements and determination of the tropospheric grid corrections with the ionospheric free phase measurements.	**Step 5:**Using ambiguity resolved WL for decimetre position estimation and the ionosphere-free phase measurements for centimetre position estimation.

To discuss the effects of the residual tropospheric errors after correction through interpolation of the tropospheric biases in the DD phase measurements, we refer to Zheng and Feng (2005), which showed results from analysis of about 130,000 Zenith Tropospheric Delay (ZTD) data points sampled from 129 IGS stations across Europe over 90 days. As shown in Fig 1, the results have strongly confirmed dependency of the interpolated ZTD errors on rover-to-base distance and random noise level. For a network with the maximum base-to-rover distance of 100 to 200 km, the maximum STD values of the interpolated residual ZTD errors lies between 10 to 17 mm. This level of errors can cause DD ranging errors of about a few centimetres, which is considered normal for the AR and centimetre positioning with ambiguity-fixed ionosphere-free observables at the user-end.

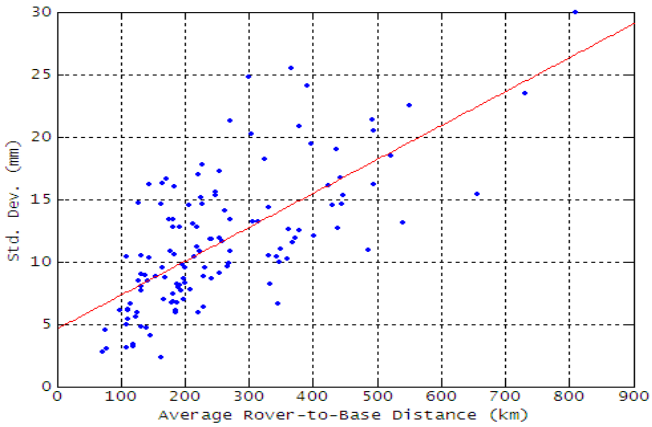

Fig 1 Residual ZTD errors versus base-rover distances through interpolation
(from Zheng and Feng, 2005)

In the future station placement, we must also consider the situations where both dual-frequency and triple-frequency receives would be used as reference station equipment together for long term. One straightforward strategy is to double the inter-station distance when triple frequency receivers are equipped with respect to the inter-station distance where the dual-frequency stations are used in a CORS network. In this placement scheme, dual-frequency receiver stations between the triple frequency stations are considered as densifications, or removable or temporary stations. Fig 2 schematically illustrates a square layout of the reference stations with dual-frequency or triple-frequency receivers. The factor of the station reduction with triple-frequency receivers is 4. However, this square layout is not ideal. As the inter-stations are non-equidistant, thus it is difficult to control of distance-dependent residual tropospheric errors. For the inter-station distance of 2d, the maximum base-rover distance can however reach 1.414d inside the network coverage, which is about 100 km when the inter-station distance is 140 km for the triple-frequency network. A more reasonable placement strategy is similar to the cell design of a cellular network, where a hexagon pattern provides for equidistant stations, which are in the centre of each coverage area as shown in Fig 3. For the inter-station distance of 2d=140 km, the maximum base-rover distance would be only 1.155d=81 km for a triple-frequency network. When the inter-station distance is increased to about 2d=180 km, the maximum base-rover distance is of 103km. This maximum base-rover distance can restrict the STD uncertainty of the interpolated residual ZTD to the level of 10 mm or so. Doubling the inter-station distance leads to the reduction of stations to a factor of 4. As a result, the number of triple-frequency stations needed to cover the inhabited Queensland areas would be reduced to 40 to 50 stations, which is much more affordable.

In the actual reference station deployment, however, it is desirable to optimally select station locations from candidate sites in a specific area to cover for given criteria of the network, such as inter-station distances. Tang et al (2007) made the first attempt for an optimal station placement scheme based on a graph-theory tool to minimize the number of stations, for a specific maximum base-rover distance and user geographical distributions. Furthermore numerical studies on the case of candidate stations being uniformly distributed may be helpful to verify the consistence between an optimal station selection result and a theoretical hexagon layout.

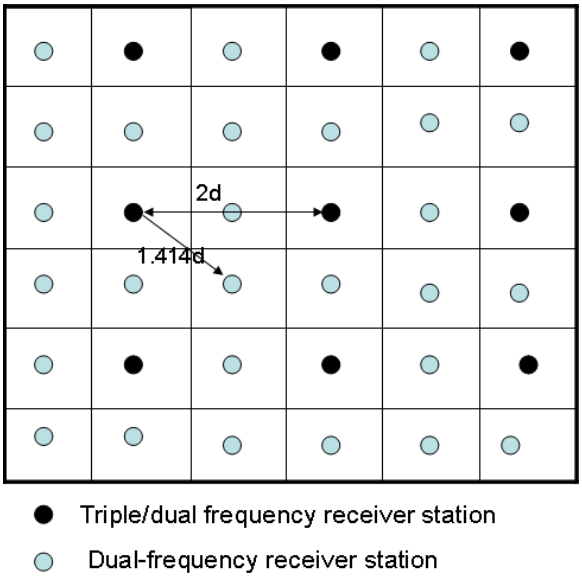

Fig 2. Square layout of reference station placement with triple and dual –frequency receives

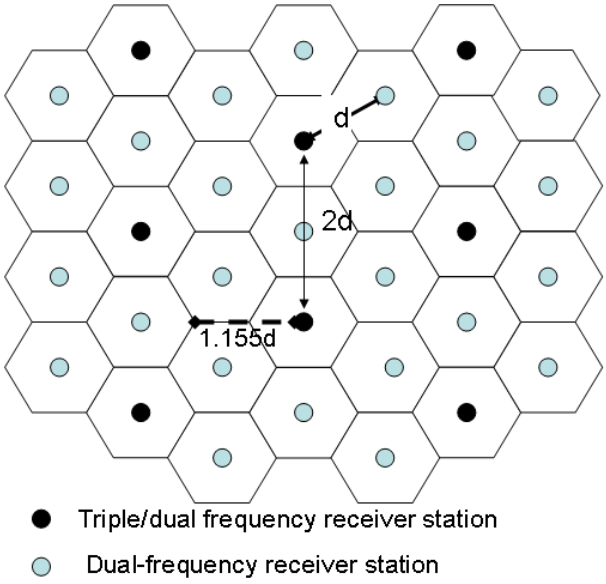

Fig 3. Hexagon layout of reference station deployment with triple and dual-frequency receivers.

4. Generation of additional carrier phase observables from dual-frequency GPS data

The above AR performance of using multiple GNSS signals sounds promising but is given in theory. The problem is that simulated GNSS data are based on operator's assumptions instead of the real world situations, for variations of different delays and magnitudes of uncertainty of different error sources. In this section, we will outline a semi-simulation approach proposed by Li (2008) for generating the third frequency DD GPS signals from the existing L1 and L2 signals, and the semi-generated data can be applied for AR and PE performance analysis purposes.

The fundamental formulae for generating DD P5 code observation and DD L5 phase observation can be described as,

$$\Delta\nabla P_5 = \Delta\nabla\rho + \Delta\nabla\delta_{trop} + \frac{f_1^2}{f_5^2}\Delta\nabla\delta I + \varepsilon_{\Delta\nabla P_5} \tag{23}$$

$$\Delta\nabla\phi_5 = \Delta\nabla\rho + \Delta\nabla\delta_{trop} - \frac{f_1^2}{f_5^2}\Delta\nabla\delta I + \Delta\nabla N_5 + \varepsilon_{\Delta\nabla\phi_5} \tag{24}$$

While the tropospheric term $\Delta\nabla\delta_{trop}$ and the ionospheric term $\Delta\nabla\delta I$ are the same as for L1 and L2 phase measurements, the DD code and phase noises noise terms $\varepsilon_{\Delta\nabla P_5}$ and $\varepsilon_{\Delta\nabla\Phi_5}$ should be generated. The phase ambiguity term $\Delta\nabla N_5$ can be set to arbitrary integer values.

The semi-simulation method includes three main steps. As shown in Eqs (23) and (24), the ionospheric delay, ambiguity and observation noise are dependent on the different frequency observables and the tropospheric error is free of frequency effects. Therefore, in order to create new frequency observation, the ionospheric delay and the tropospheric error terms must be determined separately in advance. In the first step, the integer ambiguities for L1 and L2 are fixed, just what is being done in the network-based RTK processing, and thus the DD ionospheric delay at L1 can be obtained and the DD tropospheric error terms are determined with ionosphere-free combinations. Nevertheless, both the resolved ionospheric delay and tropospheric error contain the effects of L1 and L2 phase noises and these effects must be carefully considered in generation of the third signals, in order to give the third signals with correct level of phase noises. In other words, the simulated random noised $\varepsilon_{\Delta\nabla P_5}$ and $\varepsilon_{\Delta\nabla\Phi_5}$ should include the noises introduced by ionospheric delay and tropospheric error. In the second step of semi-simulation method, a new

multiple-difference based method is used to assess the uncertainty of code and phase observations and cross-correlation between L1 and L2 phase signals for long range baselines, which are considered in generation of the random noise components in the third signals. At last, the third frequency signals are generated based on the correlation coefficient of these noises and their corresponding standard deviations (STD) obtained from the particular sets of the real dual-frequency GPS measurements.

The generation of DD L5 phase signals is, however, no longer as easy as code signal generation. In principle, the random noise must be added in the generated signals to reduce the dependence of generated signal on the original ones. The STD values of phase measurements at different frequencies are always very close to each other. However, STD of noise introduced at L5 phase by the total ionospheric and tropospheric delay is larger than STDs of DD L1 and L2 and it becomes much larger when the random noise is added. Therefore, in semi-simulation method, the filtering technique is applied to reduce the uncertainty of the total delay, notated as $W = \Delta\nabla\delta_{trop} - \frac{f_1^2}{f_5^2}\Delta\nabla\delta I$, such that its influence for DD L5 can be somehow reduced. As a result, the DD L5 signal is practically generated as,

$$\Delta\Phi_5 = \Delta\rho + \tilde{W} - \lambda_5\Delta N_5 + \varepsilon_{\Delta\nabla\Phi_5} \tag{25}$$

with $\tilde{W}$ is filtered/smoothed integrated error.

On all accounts, the semi-simulation approach is convenient and efficient for generation of new DD signals based on the existent dual-frequency GPS data sets, and the generated signals are rather consistent with the real word scenarios, and they can be used to demonstrate the network-RTK capability over longer inter-station baselines and benefit of three-frequency based GNSS technology and applications (Li, 2008).

5. Experimental Results

The purpose of numerical experiments is to demonstrate the capability of AR over long inter-station baselines as outlined in Table 2. Four RINEX GPS data sets sampled at 1 second on February 1, 2008 were collected from the US CORS (http://www.ngs.noaa.gov/CORS), and the lengths of three baselines are about 53km, 78km and 155km, respectively. Observation types for all data sets include C1, P2, L1 and L2. For each baseline, the third phase and code observables were primarily generated using the semi-simulation method as outlined in Section 4. The network-based RTK computations are completed with four steps as outlined in Table 2. Results obtained from each step are presented below.

First, we examine AR performance for the EWL observables with Eqs (16) and (17). Table 3 presents the AR success rates for different EWL observables obtained from single epoch measurements. AR success rate here is defined as the ratio of the total number of epochs when all DD ambiguities were correctly determined to the total number of epochs over the 24-h sample period. It is clear that the AR performance of the EWL observables does not show distance dependency. The slightly lower AR success rate on the 53 km baseline may reflect the effect of larger code and phase noise.

Table 3: The success rate of AR for EWL observables from single epoch

Observables	**Model**	**AR process**	**Success rate of AR (%)**		
			53km	78km	155km
$\Delta\nabla P_{(0,1,1)} - \Delta\nabla\Phi_{(0,1,-1)}$	Geometry-free Eq (16)	Rounding	100	100	100
$\Delta\nabla\Phi_{(1,-6,5)}, \Delta\nabla P_{(1,1,0)}$	Geometry-based Eq (17)	LAMBDA	99.99	100	100

As indicated in Table 2, the noise level of the estimated ionospheric delay (18) in Step 3 is amplified, and thus being smoothed with the estimate (19). For the 155km baseline, Fig 4 compares the DD ionospheric biases that are estimated from Eq (18) and smoothed with Eq (19) over a window of the most current 100 seconds and computed from the ambiguity-fixed L1 and L2 phase measurements (19), respectively. The lower panel shows the difference

between the two estimates, in the range of ± 4 centimetres, or roughly STD of less than 2 centimetres. Similar smoothing results were obtained from other baselines. This smoothing result is promising: the DD ionospheric delays can be determined to accuracy of a few centimetres over a few minutes for long baselines. This performance is possible only when the third carrier signal, e.g. L5, is available. And could extend some impact for future positioning services and applications.

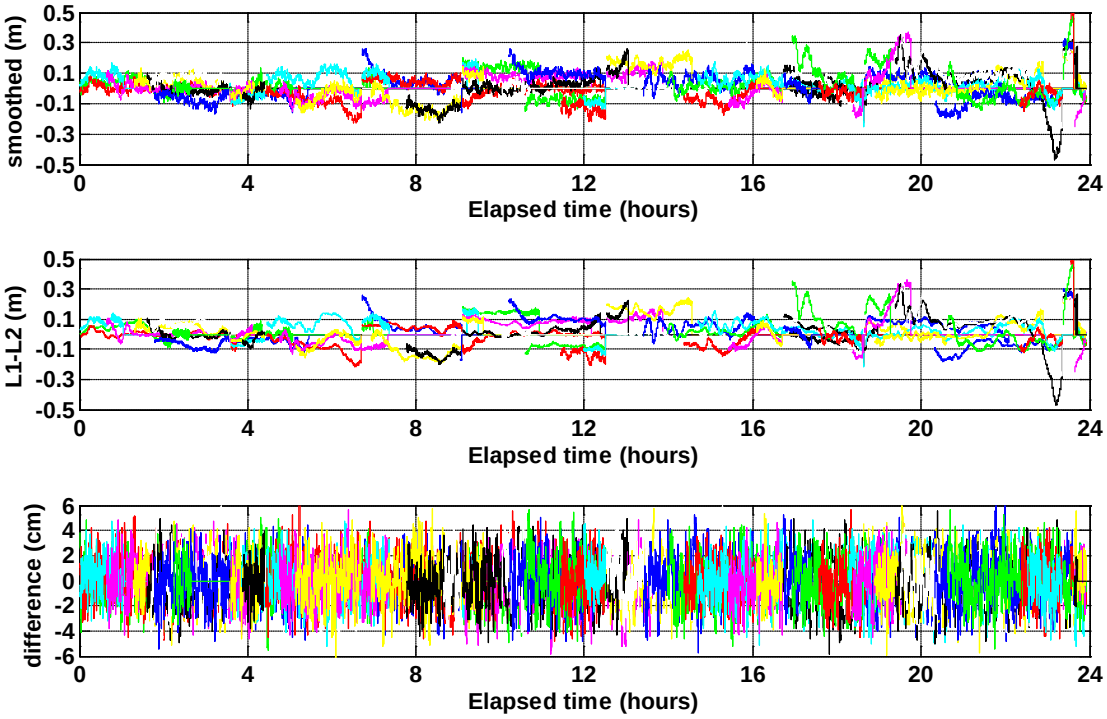

Fig 4. Illustration of the DD ionospheric estimates: accurate and smoothed over 100 seconds

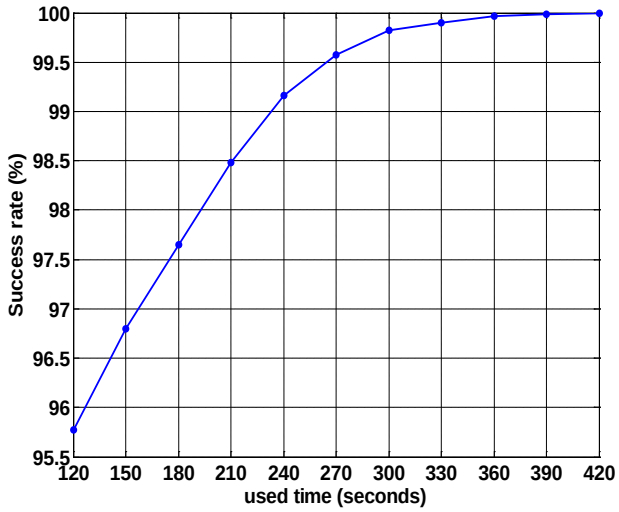

Fig 5. AR success rates of the third observable versus the averaging time

We now study the AR performance of the third observable with Eq (20) in Table 2, which is based on the smoothed ionospheric estimation in Step 3. Fig 5 plots the AR success rates of the third ambiguity versus the averaging/smoothing period for the 155 km baseline. It is observed that over about 6 to 7 minutes, the 100% AR success rate is achieved. This result shows significant performance potential for future GNSS technological evolutions and applications.

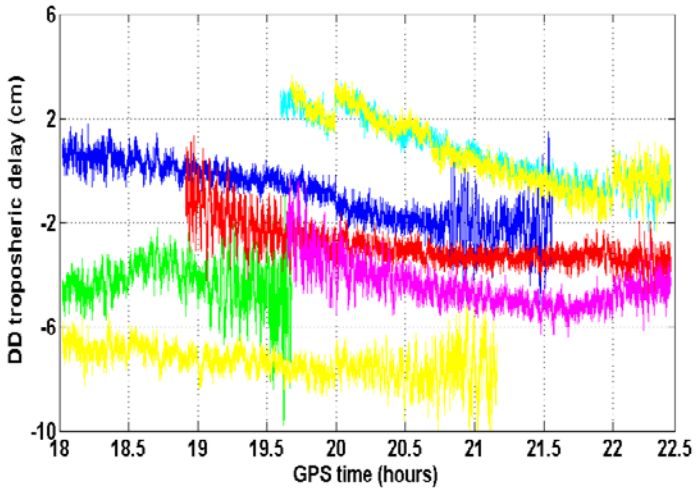

Fig 6. DD tropospheric biases estimated from ionosphere-free phase measurements (Baseline =78km)

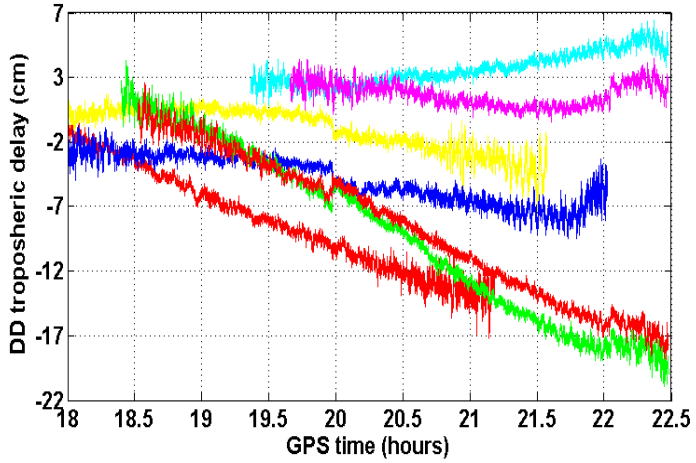

Fig 7. DD tropospheric biases estimated from ionosphere-free phase measurements (Baseline =155km)

After all ambiguities are successfully resolved, the DD tropospheric biases can be estimated with ionosphere-free phase measurements. Figs 6 and 7 show the variations of the tropospheric biases estimated for some DD pairs over a few hours, for two baselines: 78 km and 155 km, respectively. These biases must be corrected at the user locations via interpolation process to achieve centimetre positioning accuracy, which is the key for long distance RTK performance in the future.

6. Concluding remarks

The paper has outlined the geometry-free and geometry-based models that allow the ambiguities of three carriers to be resolved over the baselines of a few hundreds of kilometres between continuously operating reference stations (CORS). As a result, the key remaining limiting factor for implementation of a regional scale network RTK would be the distance-dependence of the tropospheric errors in DD phase measurements. A reference station placement scheme by doubling the inter-station distances has been proposed based on the long-range TCAR capacity and predictability of the tropospheric errors within a few hundred kilometres.

A semi-simulation procedure has been used for generation of the third GPS signals from the real GPS L1 and L2 data, in order to assess the TCAR performance benefits in the real world situations. Numerical studies performed with the 24-h data sets from 4 US CORS stations are highlighted as follows:

- 100% AR reliability of the two best EWL observables can achieve almost without distance constraints, using measurements from a single to a few epochs;
- With the two ambiguity-resolved observables, the DD ionospheric delays can be determined to centimetre accuracy within an observation period of a few minutes for long baselines.
- With the two ambiguity-resolved observables as constraints, the AR reliability of 100% for the third observable is achievable by averaging over the observation period of above 7 minutes.

The above demonstrated superior AR performance achieved with the outlined TCAR algorithms directly provides the technical basis for deployment of regional scale network RTK services with doubled inter-station distances. There is, however, no doubt that the distance-independent nature of the AR performance would have significant implications for future GNSS technological evolutions and applications.

Acknowledgements

This work was carried out with financial support from the Cooperative Research Centre for Spatial Information (CRCSI) project 1.4:- “Delivering precise positioning services in regional areas”, 2007-2010. The authors would like to acknowledge the indirect contributions from the other key researchers in the project, especially Mr Matt Higgins of Queensland Department of Nature Resources and Water, Dr Maolin Tang of Queensland University of Technology, Prof. Chris Rizos and Dr Samsung Lim of University of New South Wales.

References

Chen W., Hu C., Chen Y., Ding X. (2001), Rapid static and kinematic positioning with Hong Kong GPS active network. In: ION GPS 2001, 11-14 September 2001, Salt Lake City, UT

Cislowski G., Higgins M. (2006), SunPOZ: Enabling Centimetre Accuracy GNSS Applications in Queensland, Paper 100, Proceedings of IGNSS 2006 Symposium on GPS/GNSS, July, Gold Coast. Australia.

De Jonge P., Teunissen P., Jonkman N., Joosten P. (2000), The Distributional Dependence of the Range on Triple Frequency GPS Ambiguity Resolution, Proceedings of ION-NTM 2000, Jan 26-28, Anaheim, CA, pp 605-612.

Feng Y. (2008), GNSS Three Carrier Ambiguity Resolution Using Ionosphere-reduced Virtual Signals, Journal of Geodesy, http://dx.doi.org/10.1007/s00190-008-0209-x.

Feng Y., Rizos C. (2005), Three Carrier Approaches for Future Global, Regional and Local GNSS Positioning Services: Concepts and Performance Perspectives, Proceedings of ION-GNSS 2005, pp 2277-2787, Sept 13-16, Long Beach, CA.

Feng Y., Moody M. (2006), Improved Phase Ambiguity Resolution Using Three GNSS Signals, PCT/AU2006 /000492, http://www.wipo.int/pctdb, April 2006.

Feng Y., Rizos C. (2007), Geometry-based TCAR Models and Performance Analysis, Presented at IUGG2007, July 2-13, Perugia, Italy, and accepted for publication in the IAG proceedings.

Feng Y., Rizos C., Higgins M. (2007), Multiple Carrier Ambiguity Resolutions and Performance Benefits for RTK and PPP in Regional Areas, Proceedings of ION-GNSS 2007, pp 668-678, Sept 25-28, Fort Worth, TX.

Forssell B., Martin-Neira M., Harris R. (1997), Carrier Phase Ambiguity Resolution in GNSS-2. Proceedings of ION-GPS 1997, pp 1727-1736, Sept 16-19, Kansas City, MO.

Han S., Rizos C. (1999), The Impact of Two Additional Civilian GPS Frequencies on Ambiguity Resolutions Strategies, Proceedings of ION Annual Technical Meeting, pp 315-321, June 28-30, Cambridge, MA.

Hatch R., Jung J., Enge P., Pervan B. (2000), Civilian GPS: The Benefits of Three Frequencies, GPS Solutions, Vol 3, No 4, pp 1-9.

Hatch R. (2006), A New Three-Frequency, Geometry-Free Technique for Ambiguity Resolution, Proceedings of ION-GNSS 2006, pp 309-316, Sept 26-29, Fort Worth, TX.

Henkel P, Cünther C. (2007) Integrity Analysis of Cascaded Integer Resolution with Decorrelation Transformations, Proceedings of the Institute of Navigation, National Technical Meeting, San Diego

Kim Don, Langley Richard B. (2007) Long-Range Single-Baseline RTK for Complementing Network-Based RTK, Proceedings of ION GNSS 2007, pp 639-650, Sept 25-28, Fort Worth, Texas

Li B. (2008), Generation of the Third Code and Phase GPS Signals Based on Dual-Frequency GPS Measurements, ION GNSS 2008, savannah Georgia, 16-19 September, (accepted as a sponsored student paper)

Rizos C., Han S. (2003), Reference Station Network Based RTK Systems - Concepts & Progress, Wuhan University Journal of Nature Sciences, 8(2B), pp 566-574.

Tang M., Feng Y., Burnett L., Hayward R., Raymond K. (2007), A Reference Station Placement Scheme in Deployment of Network Real-Time Kinematic Positioning Systems, Proceedings of IGNSS 2007, Paper 123, 4-6 December, Sydney, 2007.

Teunissen P., Joosten P., Tiberius C. (2002), A comparison of TCAR, CIR and LAMBDA GNSS ambiguity resolution. In: Proceeding of ION GPS, 24-27 Sept. Portland, Oregon, pp 2799-2808

Vollath U., Birnbach S., Landau H. (1998), Analysis of Three Carrier Ambiguity Resolution (TCAR) Technique for Precise Relative Positioning in GNSS-2, Proceedings of ION-GPS 1998, Sept., pp 417-426.

Vollath U. (2004), The Factorized Multi-Carrier Ambiguity Resolution (FAMCAR) Approach for Efficient Carrier-Phase Ambiguity Estimation, Proceedings of ION-GNSS 2004, pp 2499-2508, Sept 21-24, Long Beach, CA.

Zhang J., Lachapelle G. (2001), Precise estimation of residual tropospheric delays using a regional GPS network for real-time kinematic applications, Journal of Geodesy, 75: 255-266.